# Multiscale neuro-inspired models for interpretation of EEG signals in patients with epilepsy

Fabrice Wendling, Elif Koksal-Ersoz, Mariam Al Harrach, Maxime Yochum, Isabelle Merlet, Giulio Ruffini, Fabrice Bartolomei, Pascal Benquet

▶ **To cite this version:**

Fabrice Wendling, Elif Koksal-Ersoz, Mariam Al Harrach, Maxime Yochum, Isabelle Merlet, et al.. Multiscale neuro-inspired models for interpretation of EEG signals in patients with epilepsy. Clinical Neurophysiology, 2024, 161, pp.198-210. ⟨10.1016/j.clinph.2024.03.006⟩. ⟨hal-04533986⟩

**HAL Id: hal-04533986**

**https://hal.science/hal-04533986v1**

Submitted on 27 Mar 2026

**HAL** is a multi-disciplinary open access archive for the deposit and dissemination of scientific research documents, whether they are published or not. The documents may come from teaching and research institutions in France or abroad, or from public or private research centers.

L'archive ouverte pluridisciplinaire **HAL**, est destinée au dépôt et à la diffusion de documents scientifiques de niveau recherche, publiés ou non, émanant des établissements d'enseignement et de recherche français ou étrangers, des laboratoires publics ou privés.

Distributed under a Creative Commons CC BY-NC-ND 4.0 - Attribution - Non-commercial use - No Derivative Works - International License

Clinical Neurophysiology 161 (2024) 198–210

Contents lists available at ScienceDirect

Clinical Neurophysiology

journal homepage: www.elsevier.com/locate/clinph

# Multiscale neuro-inspired models for interpretation of EEG signals in patients with epilepsy

Fabrice Wendling [a,1,*], Elif Koksal-Ersoz [a,1], Mariam Al-Harrach [a,1], Maxime Yochum [a], Isabelle Merlet [a], Giulio Ruffini [b], Fabrice Bartolomei [c,d], Pascal Benquet [a,1]

[a] Univ Rennes, INSERM, LTSI – U1099, Rennes, France
[b] Neuroelectrics, Barcelona, Spain
[c] APHM, Timone Hospital, Epileptology and Cerebral Rhythmology Department, Marseille, France
[d] Univ Aix Marseille, INSERM, INS, Inst Neurosci Syst, Marseille, France

## HIGHLIGHTS

- Neuro-inspired computational models of human cortex developed at three levels (cellular, assembly and whole brain) are described.
- Models explain the cell- and network-related mechanisms underlying the generation of i) fast ripples and ii) SEEG- and EEG-recorded epileptic spikes and spike-waves.
- The knowledge gained from these models effectively complements the clinical analysis of SEEG data collected during the evaluation of patients with epilepsy.

## ARTICLE INFO

*Article history:*
Accepted 11 March 2024
Available online 16 March 2024

*Keywords:*
Epilepsy
Brain
Computational modeling
Microscale
Mesoscale
Largescale
EEG
SEEG
Interictal activity
Spikes
Spike-waves
Fast ripples

## ABSTRACT

*Objective:* The aim is to gain insight into the pathophysiological mechanisms underlying interictal epileptiform discharges observed in electroencephalographic (EEG) and stereo-EEG (SEEG, depth electrodes) recordings performed during pre-surgical evaluation of patients with drug-resistant epilepsy.
*Methods:* We developed novel neuro-inspired computational models of the human cerebral cortex at three different levels of description: i) microscale (detailed neuron models), ii) mesoscale (neuronal mass models) and iii) macroscale (whole brain models). Although conceptually different, micro- and mesoscale models share some similar features, such as the typology of neurons (pyramidal cells and three types of interneurons), their spatial arrangement in cortical layers, and their synaptic connectivity (excitatory and inhibitory). The whole brain model consists of a large-scale network of interconnected neuronal masses, with connectivity based on the human connectome.
*Results:* For these three levels of description, the fine-tuning of free parameters and the quantitative comparison with real data allowed us to reproduce interictal epileptiform discharges with a high degree of fidelity and to formulate hypotheses about the cell- and network-related mechanisms underlying the generation of fast ripples and SEEG-recorded epileptic spikes and spike-waves.
*Conclusions:* The proposed models provide valuable insights into the pathophysiological mechanisms underlying the generation of epileptic events. The knowledge gained from these models effectively complements the clinical analysis of SEEG data collected during the evaluation of patients with epilepsy.
*Significance:* These models are likely to play a key role in the mechanistic interpretation of epileptiform activity.
© 2024 International Federation of Clinical Neurophysiology. Published by Elsevier B.V. This is an open access article under the CC BY-NC-ND license (http://creativecommons.org/licenses/by-nc-nd/4.0/).

*Abbreviations:* EEG, electroencephalography; SEEG, stereoelectroencephalography; EZ, epileptogenic zone; PZ, propagation zone; NEZ, non-epileptogenic zone; EI, epileptogenic index; NMM, neural mass model; IEDs, interictal epileptiform discharges; FRs, fast ripples; SWs, spike-wave; ESs, epileptic spikes; PYR cells, pyramidal cells; INs, interneurons; GLU, glutamate; PSCs, Post Synaptic Currents; AMPA, α-amino-3-hydroxy-5-methyl-4-isoxazolepropionic acid; NMDA, N-methyl-D-aspartate; GABA, gamma-aminobutyrique acid; SST+, somatostatin positive; PV+, parvalbumin positive; VIP+, vaso-intestinal peptide positive; NGFC, Neuroglial form cells; BIS, bistratified; OLM, oriens-lacunosum-moleculare; BAS, basket; CA1, cornu Ammonis subfield 1; CA3, cornu Ammonis subfield 3.

* Corresponding author at: LTSI, Inserm U1099 - Université de Rennes, Campus de Beaulieu - Bât. 22, 35042 Rennes, France.
*E-mail address:* fabrice.wendling@inserm.fr (F. Wendling).
[1] Equal contribution.

https://doi.org/10.1016/j.clinph.2024.03.006
1388-2457/© 2024 International Federation of Clinical Neurophysiology. Published by Elsevier B.V.
This is an open access article under the CC BY-NC-ND license (http://creativecommons.org/licenses/by-nc-nd/4.0/).

## 1. Introduction

Epilepsy refers to a group of neurological disorders characterized by recurrent seizures during which brain activity becomes abnormal, resulting in aberrant motor manifestations and/or sensory and behavioral abnormalities with possible loss of awareness (El Youssef et al., 2022). This complex dynamic disorder involves pathophysiological neuronal alterations of brain networks that occur at the microscopic (subcellular) to the macroscopic level (interconnected neuronal assemblies distributed in distant regions). These alterations result in two major abnormal mechanisms specific to epileptogenic networks: hyperexcitability and hypersynchronization (Aronica and Muhlebner, 2017).

The main mechanisms identified so far include, but are not limited to, increased excitability at the level of principal pyramidal cells (PCs), due to modifications of transmembrane ion channels (Na+ (Catterall, 2012), K+ (Levesque and Avoli, 2019)), upregulation of glutamatergic (Colciaghi et al., 2014) receptors such as NMDA (Naylor et al., 2013) receptors or dysregulation of chloride co-transporters (KCC2 (Belperio et al., 2022), NKCC1 (Liu et al., 2019)). Synchronization is amplified by increased collateral glutamatergic excitation (Hedrick et al., 2017) and/or reorganizations at the level of GABAergic interneurons (INs), leading to a deficit of inhibitory input to PCs (Cossart et al., 2005). The pathophysiological mechanisms are both structural (such as cell loss (Swartz et al., 2006)) and functional (such as changes in postsynaptic currents (PSCs) (Dichter, 1989)). At the network level, many studies have found alterations in glutamatergic (GLU) synaptic AMPA and extrasynaptic NMDA receptors, which play a key role in the plasticity of excitatory synapses (review in (Casillas-Espinosa et al., 2012)). Previous studies have also found similar results regarding GABAergic synaptic transmission. They reported a mechanism of disinhibition caused by depolarizing GABA related to chloride overload through GABAa receptors (Burman et al., 2019, Staley, 2004), which is explained by the dysregulation of chloride transporters (Huberfeld et al., 2007). In the epileptic tissue, changes also occur i) in the extracellular space where the increase in K + concentration has multiple excitatory effects (de Curtis et al., 2018), ii) in non-synaptic neuronal couplings (ephaptic interactions or gap junctions (review in (Nemani and Binder, 2005))) which enhance synchronization, and iii) in astrocyte function that controls the balance between GLU release and uptake (Volman et al., 2012).

In the context of epilepsy, one of the main challenges arises from the fact that the multifaceted mechanisms mentioned above are not mutually exclusive. They can act "in synergy," making it difficult to interpret electrophysiological signals recorded at various spatial scales, from intracellular activity to local field potentials and to (stereo)electroencephalography in humans.

This complexity can be addressed by using neural computational modeling, which is recognized as the most efficient way to integrate structural, functional, and dynamical properties of neural systems into "coherent and interpretable views" (Suffczynski et al., 2006). Indeed, computational models offer an efficient way to structure new and detailed knowledge coming from neurobiological research. They are useful for interpreting both experimental results (Case and Soltesz, 2011, Gentiletti et al., 2022, Wei et al., 2023) and clinical data recorded during interictal or ictal episodes (Makhalova et al., 2022, Sinha et al., 2017). Computational models also have the unique ability to formalize and relate variables across multiple levels of analysis, offering the possibility to link between successive levels of reduction.

The objective of this study is to highlight the advantages of using a multiscale modeling approach to interpret electroencephalographic (EEG) and stereo-EEG (SEEG) data recorded during pre-surgical evaluation of drug-resistant patients who are candidates for surgery in order to identify a hypothesized epileptogenic zone (EZ). The motivation behind accurate modeling of neuronal cells and networks, based on relevant biophysical and neurophysiological data, is to make mechanistic hypotheses about the nature of epileptiform markers observed in (S)EEG signals.

The models described here integrate up-to-date neurophysiological knowledge into parametrized mathematical nonlinear dynamical systems which consist of coupled differential equations. The parameters in these systems have a direct interpretation in terms of the underlying neurobiological and/or neurophysiological processes. These models were designed to accurately replicate electrophysiological epileptiform patterns observed during ictal (seizure) and interictal (non-seizure) periods. This study specifically focuses on interictal epileptic discharges that include transient interictal events such as mono-/multi-phasic spikes or polyspikes, spike-waves, and high-frequency oscillations like ripples [80–200 Hz] or fast ripples [200–600 Hz]. The presented models effectively complement the visual inspection of SEEG and EEG signals, thereby significantly improving their diagnostic value.

## 2. Materials and methods

### 2.1. SEEG and EEG recordings

Typical examples of epileptiform activity were selected by visual inspection of recordings performed in the Epilepsy Surgery Unit of La Timone University Hospital, Marseille, France. This data subset was extracted from a larger database (n = 50 patients) collected for the project named "EEG-Process" ("Retrospective analysis of EEG signals collected in routine care during the evaluation of epileptic patients"), which was approved by legal entities including the Institutional Review Board (IRB00003888, IORG0003254, FWA00005831) of the French Research Institute for Health and Medical Research (Inserm). According to our clinical practice, SEEG and EEG recordings are performed as part of the normal clinical care of patients who give informed consent. Patients are informed that their data may be used for research purposes.

SEEG signals are recorded during long-term video-SEEG monitoring (5 to 8 days) using intracerebral multiple lead electrodes placed intracranially according to Talairach's stereotactic method (Bancaud et al., 1970) and French guidelines (Isnard et al., 2018). Electrode placement is determined for each patient based on available non-invasive information and hypotheses about the patient-specific localization of the epileptogenic zone. The accuracy of the implantation is peroperatively monitored by telemetric x-ray imaging. A post-operative CT scan without contrast product is then used to verify both the absence of bleeding and the precise 3D location of each electrode contact. After SEEG exploration, intracerebral electrodes are removed. A CT scan/MRI data fusion is performed to anatomically locate each contact along each electrode trajectory.

For the purpose of this study, analyzed SEEG signals were selected from patients with electrode contacts positioned in limbic (hippocampus, microscale modeling) or in neocortical regions (meso- and large-scale modeling). Signals were recorded on a Deltamed-NatusTM system on a maximum number of channels equal to 256, sampled at 2048 Hz or 1024 Hz depending on the modeled epileptiform SEEG pattern (high-frequency oscillations or epileptic spikes). A hardware analog high-pass filter (cutoff frequency equal to 0.16 Hz) was present in the recording system to remove very slow oscillations of the baseline. An example of intracerebral SEEG exploration in temporal lobe epilepsy (TLE) is described in section 3.2.

Scalp EEG signals were selected from a patient who also underwent a SEEG exploration. They were recorded on a 32-channel system according to standard clinical practice.

### 2.2. Neuro-inspired microscale computational model of hippocampus for analysis of epileptic high frequency oscillations (HFOs)

HFOs have been a topic of increasing interest over the last twenty years (Staba et al., 2014) (Jiruska et al., 2017). They are observed in both epileptic and non-epileptic brain regions (Pail et al., 2020). Here, we focus on a particular type of pathological HFOs recorded from the human hippocampus (Fig. 1.A1). These HFOs are called fast ripples (FRs) because they are brief (a few tens of milliseconds) signals that occur in a specific EEG frequency band (200–600 Hz) (Fig. 1.A2).

Seminal studies reported the presence of FRs in experimental *in vivo* models of epilepsy (rat, kainate models) (Bragin et al., 1999c) as well as in the human epileptic brain (SEEG recording from hippocampus and entorhinal cortex) (Bragin et al., 1999a). Since then, their clinical value has been confirmed by numerous studies (Jacobs et al., 2009, Urrestarazu et al., 2007) (Cuello-Oderiz et al., 2018, Weiss et al., 2021).

To gain insight into the mechanisms of generation of interictal FRs observed in SEEG signals recorded in patients with TLE during pre-surgical evaluation, we developed a 3D neuronal network model of the anterior part of the hippocampus. This choice was motivated by the frequent observation of FRs in this region of the limbic system. This physiologically and biophysically plausible computational model mimics the CA1 subfield of the hippocampus (Fig. 1.B). It is an original model adapted from a previous model developed by Demont-Guignard and colleagues (Demont-Guignard et al., 2012). In this updated version, we introduced a biophysical model of the electrode-tissue interface (ETI) and incorporated the possibility of changing the electrode geometry (size and orientation) (Fig. 1.C). Briefly, the model consists of a detailed network of principal neurons (pyramidal -PYR- cells) connected to three different types of interneurons: basket cells (BAS) which target PYR cell somata and oriens-lacunosum-moleculare (OLM) and bistratified (BIS) cells which target PYR cell dendrites (Fig. 1.D). These cells were synaptically interconnected, respecting the known features of hippocampal cytoarchitecture (Adler et al., 2012, Romani et al., 2022). A reduced two-compartment model ((Demont-Guignard et al., 2009), Figure A.1, Appendix A) and a single-compartment model (adapted from (Hajos et al., 2004)) were used for the excitatory PYR cells and the inhibitory interneurons, respectively.

Different types of somatic and dendritic ion channels were included in these compartments because of their potential role in epilepsy (Demont-Guignard et al., 2009). Each neuron subtype contained different classes of voltage-gated, ligand-gated, and leak channels, allowing the neuron models to generate realistic firing patterns. Cell membrane properties were expressed using the Hodgkin-Huxley formalism. Dipole theory was used to calculate the local field potential (LFP), based on the well-established assumptions that i) PYR cells function as current dipoles that are the main contributors to the LFP and ii) the surrounding extracellular space is homogeneous. For a detailed description of the microscale model, readers may refer to Appendix A. It is worth noting that this cellular level of modeling is motivated by the need to have an explicit representation of action potentials (APs) to simulate FRs as originally reported in (Ibarz et al., 2010). Furthermore, the combination of the neurophysiological model with models of electrode geometry and ETI is novel. This allowed us to i) explain the diversity of FR waveforms and corresponding spectral features and ii) account for brain tissue changes due to gliosis.

### 2.3. Neuro-inspired mesoscale multilayer computational model for analysis of interictal epileptiform discharges (IEDs) in neocortical brain regions

The mesoscale model described here and the microscale model described above were developed separately because they correspond to different cortical structures, i.e., a mesoscale model for the neocortex and a microscale model for the hippocampus. Therefore, the mesoscale model was not directly derived from the microscale model.

Over the past decades, IEDs have been extensively studied in the field of epilepsy ((de Curtis and Avanzini, 2001), review in (de Curtis et al., 2012)). IEDs refer to a wide variety of electrophysiological markers ranging from simple isolated monophasic spikes to more complex events, including biphasic spikes or spike-waves, polyspikes, and bursts (Keller et al., 2010). Spike-waves (SWs) are frequently observed in SEEG recordings not only in limbic structures but also in neocortical regions. Recent studies suggest that SWs may be predictive of seizure onset and seizure propagation zone (Cuello-Oderiz et al., 2018, Koksal-Ersoz et al., 2022, Thomas et al., 2023).

To explain these findings, we developed a novel layered model of the human neocortex. This model follows the neuronal population approach first proposed by Wilson and Cowan (Wilson and Cowan, 1972) and developed in neurophysiology by Freeman to study the olfactory system (Freeman, 1978) and by Lopes da Silva to understand the genesis of the EEG alpha rhythm (Lopes da Silva et al., 1974).

The mesoscale neural mass model (NMM) presented here builds on neuronal population models previously developed in our group (Mina et al., 2013, Molaee-Ardekani et al., 2010, Wendling et al., 2002). The novelty is that it takes into account the layered cytoarchitecture of the neocortex as superficial and deep layers are known to play a role in the generation of interictal epileptiform discharges in the human neocortex (Fabo et al., 2023). To our knowledge, only two recent studies (Lopez-Sola et al., 2022, Sanchez-Todo et al., 2023) have used a similar approach in a different context to i) propose a modeling framework to decipher the circuitry underlying brain oscillations and ii) bridge between different types of electrophysiological measurements.

A detailed description of the mesoscale model is given in Appendix B. A summary of the main features is given here. The model is designed to reproduce the dynamics of the average activity of a neuronal population consisting of synaptically connected neuronal subpopulations of glutamatergic excitatory neurons and inhibitory GABAergic INs. As shown in Fig. 2.A, excitatory neurons correspond to PYR cells spanning layers I to V. The model considers four types of GABAergic INs (parvalbumine + cells, PV + INs; somatostatin + cells, SST + INs; neurogliaform cells, NGFC INs; vaso-intestinal peptide-expressing cells, VIP + INs), thus integrating more neuron types than in models previously proposed (Mina et al., 2013, Molaee-Ardekani et al., 2010) as well as positions of synapses across layers. The connectivity among neuronal subpopulations (including both feedback and feedforward connections) was based on data reported in the literature (Eyal et al., 2018, Markram et al., 2015) and on the comprehensive review of interlaminar connections in the neocortex by Thomson and Bannister (Thomson and Bannister, 2003).

According to the NMM formalism, in each subpopulation, a dynamic linear transfer function converts presynaptic information (i.e., the average pulse density of afferent action potentials) into an average membrane postsynaptic potential (PSP), which can be either excitatory (EPSP) or inhibitory (IPSP). The kinetics (rise and decay times) of PSPs reproduce those of actual GLU, $GABA_{a,fast}$ and $GABA_{a,slow}$ PSPs (see Appendix B, Table B.1). In turn, a static nonlinear function (sigmoid shape) relates the average membrane

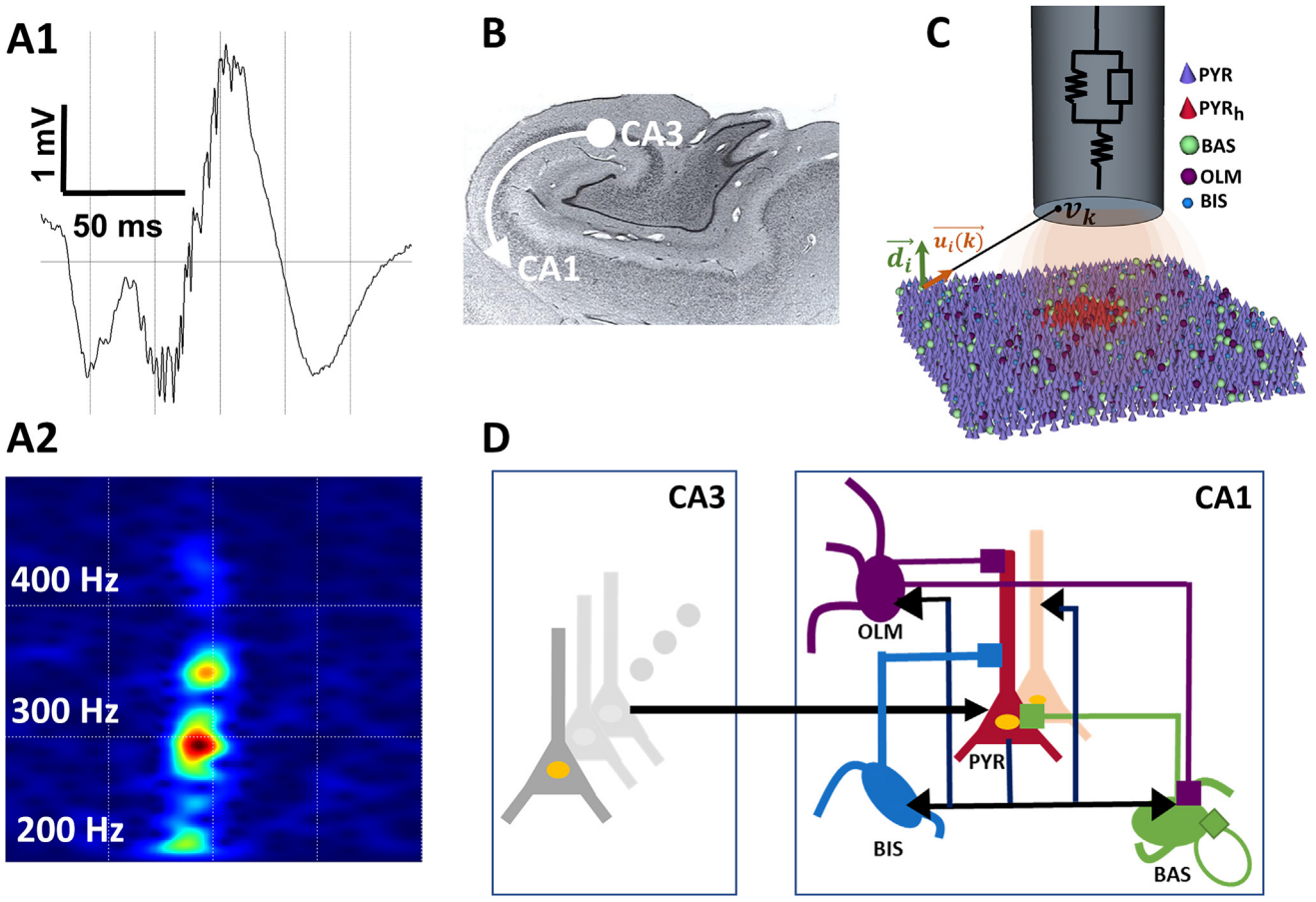


**Fig. 1.** Microscale computational model of hippocampus for simulation of epileptic high frequency oscillations (HFOs). A) Example of a real HFO (fast ripple frequency band, [200–600 Hz]) recorded from hippocampus during SEEG. B) Human hippocampal slice (adapted from (Touretzky, 2019)). The model simulates local field potentials (LFPs) generated in the CA1 subfield in response to excitatory input from the CA3 subfield via the Schaffer collaterals. C) The simulated 3D volume designed to generate CA1 network activity from interconnected pyramidal (PYR) cells and hyperexcitable PYR (PYRh) cells (n = 6991) in addition to Basket (BAS, 477), Oriens-Lacunosum Moleculare (OLM, 477), and Bistratified (BIS, 477) interneurons (INs). The Electrode-Tissue Interface (ETI) model allows accurate consideration of the extracellular electrode characteristics (impedance, size, position). D) Schematic diagram of the two connected subfields CA3 and CA1 (arrows: glutamatergic synapses, squares: GABAergic synapses). PYR cells were represented by a two-compartment (soma, dendrite) neuron model while INs were represented by a single-compartment model (details in Appendix A, Figure A.1). CA3 was simply represented as an array PYR cells firing volleys of action potentials on CA1 PYR cells. The simulated LFP was considered to be the summation of extracellular electric potentials generated by CA1 PYR cells, assumed to behave as elementary current dipoles.

potential of a given subpopulation to an average pulse density representing the sum of action potentials fired by neurons. It is worth noting that PSP amplitudes are key parameters of the model. Their values determine the excitatory/inhibitory drive of afferent inputs to a given subpopulation. Thus, they contribute significantly to the global excitation/inhibition balance of the whole neuronal population. To reconstruct the local field potential recorded by SEEG electrode contacts, we considered two synaptic locations (apical and basal) on the PYR population (layer I and layer V). As shown in Fig. 2.B, the transmembrane current caused by an apical synaptic input generates a basal return current, and the transmembrane current caused by a basal synaptic input generates an apical return current (Lopes da Silva, 2011, chapter 5). Therefore, in order to approximate the LFP recorded at the electrode contact, we considered the contribution of both synaptic current sinks and sources, simulated by two monopoles in opposite directions (Fig. 2.B).

### *2.4. Neuro-inspired large-scale computational model of the human brain for interpretation of scalp EEG signals recorded in patients with epilepsy*

In recent decades, a large body of evidence has accumulated showing that epilepsy is a disorder of brain networks, with changes occurring at both structural (Lariviere et al., 2022) and functional (Bartolomei et al., 2017) levels. It is widely accepted that epileptic mechanisms result from dysfunctional changes that occur not only in brain tissue but also in the connectivity of distant regions (Parker et al., 2018). It is also known that these dysfunctional changes are at the origin of patient-specific epileptiform abnormalities observed in electrophysiological signals (SEEG, EEG) recorded during interictal and ictal periods (Binnie and Stefan, 1999). Relating electrophysiological markers to pathological changes in epileptogenic networks (ENs) is a complex task especially in the case of scalp EEG signals which convey information about the simultaneous activity of brain sources projecting onto electrodes positioned on the head (Cosandier-Rimele et al., 2010). To fill this gap, we developed a large-scale computational model of the human brain capable of accurately simulating EEG signals recorded in patients with focal epilepsy involving of neocortical regions.

A detailed description of the macroscale model is provided in Appendix C. Key features are described below. The model is based on a previously published model (Bensaid et al., 2019) that we developed to explain features (rhythms, topography) of scalp EEG signals recorded from normal subjects during sleep and wakefulness conditions and from patients with disorders of consciousness. In this previous study (Bensaid et al., 2019), we presented a physiologically grounded computational model, that takes into account the interregional circuitry of the human cortex. The model

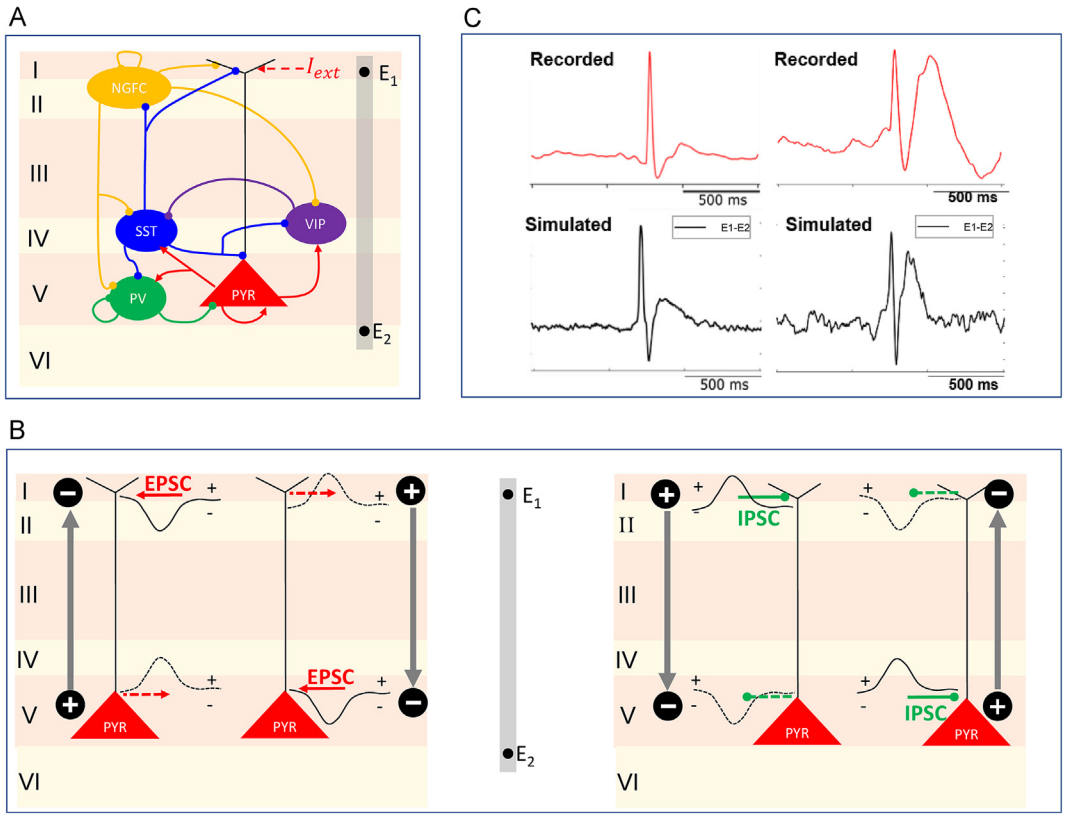


**Fig. 2.** Mesoscale laminar computational model. A) The model follows the neural mass modeling formalism (see text for details) extended by a physical model accounting for the electrical current conduction. B) To reconstruct the local field potential (LFP) recorded by the intracerebral electrode contacts (E1 and E2), two current monopoles of opposite direction are used to account for transmembrane current flow patterns that depend on the type of the input current (EPSC, left subplot or IPSC, right subplot) and on the synapse location (basal, layer 5 or apical, layer 1). The grey arrows represent the current flow in the extracellular space. For instance (B, left), an EPSC arising at the level of basal dendrites results in an active sink in the extracellular space close to this synapse and a passive source at the level of apical dendrites. These sink/source configurations in the extracellular space give rise to monopoles, whose activity is projected onto the electrode contacts. C) Illustrative examples of recorded and simulated monophasic spikes and biphasic spike waves.

consisted of a network of interconnected neocortical regions, whose activity was simulated by a NMM that accounted for the specificities of each neuronal type. A specific NMM was added to simulate thalamic activity. The global architecture included thalamocortical (vertical) and cortico-cortical (horizontal) connectivity based on the human connectome (Van Essen and Marcus, 2023). Distant neuronal assemblies could communicate through feedforward and feedback synaptic excitation and inhibition.

For the present study, the brain model was adapted to the context of epilepsy. The new model and the pipeline we developed to optimize the parameters are shown in Fig. 3.

Firstly, in order to simulate the activity of neocortical regions, the previous generic NMM was replaced by the mesoscale multilayer computational model (Fig. 3.A) described in Section 2.3 and detailed in Appendix B. Secondly, the structural connectivity (Fig. 3.B) between ROIs was based on neuroimaging data (DTI) collected and averaged from 215 subjects as provided by the Human Connectome Project (Van Essen and Marcus, 2023), whereas in our previous model it was taken from (Hagmann et al., 2008) where it was estimated from five healthy volunteers. Thirdly, for the source activity, the patient's 3D MRI data were used to reconstruct a high-resolution mesh of their cerebral cortex (Fig. 3.C). The atlas (Desikan et al., 2006) used for the anatomical parcellation of the cerebral cortex included 82 regions of interest (ROIs), whereas the previous large-scale model contained only 66 ROIs (Fig. 3.C). On this mesh, we delineated the EZ, the PZ and the "healthy" brain regions (Fig. 3.D), and we solved the EEG forward problem (using the dipole theory, see Appendix C) to project the activity of sources onto electrodes positioned on the patient's head (Fig. 3.E). An iterative parameter optimization process was then applied to simulate scalp EEG signals similar to those recorded in the patient (Fig. 3.F and 3.G).

## 3. Results

We present the results obtained at the three modeling scales. For each scale, the simulation parameters were determined from visual inspection of real (S)EEG signals recorded in patients with epilepsy. When the simulated signals reproduced the real signals with a high degree of fidelity, the models were then used to generate mechanistic insights.

### *3.1. Microscale modeling explains the mechanisms underlying FRs observed in SEEG signals*

In this section, we report simulation results obtained from the microscale model regarding the generation of fast ripples (FRs) as observed in SEEG signals recorded from an intracerebral electrode positioned in the hippocampus.

A typical FR event is shown at the top of Fig. 4.A. As depicted, FRs are short-duration (30 ms) transient events characterized by high-frequency, low-amplitude activity superimposed on a slower, higher-amplitude wave. Time-frequency analysis (spectrogram,

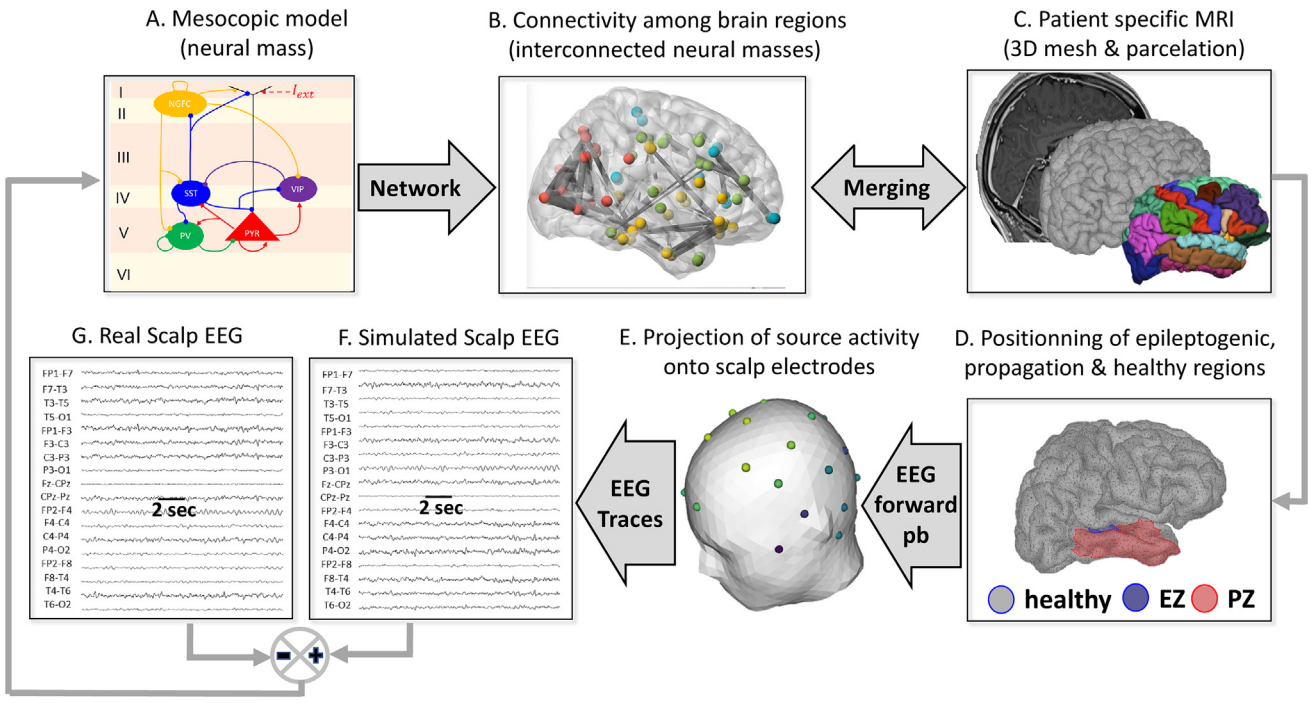


**Fig. 3.** Large-scale modeling pipeline and parameter optimization based on the comparison of simulated and real EEG signals. A) The neocortical mesoscale model (see section 2) is used to build a B) large scale network of 82 interconnected neural masses simulating the local electrophysiological activity of 82 distributed brain regions interconnected according to data provided by the Human Connectome Project. C) Neural activity is then mapped onto a high-resolution 3D mesh (obtained from patient-specific MRI data) for which a parcellation is defined based on a modified version of the Desikan-Killiany atlas (increased from 66 to 82 regions of interest). D) Healthy, epileptogenic and propagation zones (EZ and PZ, respectively) are then refined and mapped to corresponding nodes of the network generating background activity and epileptic spikes. E) By solving the EEG forward problem, the activity at the source level (neocortex) is then projected onto 32 scalp electrodes positioned on the head in order to obtain F) simulated EEG signals. G) An iterative procedure aimed at minimizing the distance between real and simulated EEG signals (in terms of amplitude, spike topography and polarity) is used to adjust model parameters (excitability, connectivity, position and extent of regions of interest).

Fig. 4.A, bottom) of this typical FR revealed that the high-frequency components (>200 Hz) were located into two subbands (around 220 Hz and 320 Hz), which is similar to previous reports in early *in vivo* studies (Bragin et al., 1999c) and later confirmed in humans (Bragin et al., 1999b, Jacobs et al., 2009, Jiruska et al., 2017). As shown in Fig. 4.B (top right), with appropriate tuning of parameters, the model captured key features of real FRs, such as the temporal profile and the presence of both low- and high-frequency components. This agreement between simulated and real FRs is also quantified by the spectrogram (Fig. 4.B, bottom).

A major advantage of the model is that it can simulate not only the local field potential (LFP) generated by the hippocampal neuronal network but also the firing patterns of individual neurons of the network (excitatory PYR cells and inhibitory BIS, OLM, BAS INs). It is worth noting that the simultaneous recording of these cell types would be very difficult to achieve experimentally. As displayed in Fig. 4.C, these firing patterns provided insight into the mechanisms involved in the generation of the FR waveform. The high-frequency component (around 300 Hz) is explained by weakly synchronized action potentials (APs) generated by small clusters of pyramidal neurons that were rendered hyperexcitable (PYRh, characterized by increased conductance associated with glutamatergic currents, decreased conductance associated with GABAergic currents and increased GABA reversal potential) as compared to "normal" PYR cells (see Fig. 1.C). Regarding the low-frequency component of the FR event, the model revealed that it is caused by an activation of the loop between PYR cells and BIS INs in response to the afferent volley of action potentials coming from CA3 (Fig. 4.C).

### *3.2. Mesoscale modeling explains the time course of SEEG-recorded spike-waves and predicts seizure onset and propagation zones*

In this section, we illustrate the ability of the mesoscale model to accurately reproduce IEDs with different morphologies, such as epileptic spikes and spike-waves recorded during presurgical evaluation of a patient suffering from lateral temporal lobe epilepsy.

During this SEEG exploration, eleven multichannel depth EEG electrodes (Fig. 5.A, B) were used to explore left temporal, orbitofrontal and parietal regions (mesial and lateral) in addition to a focal cortical dysplasia located in the temporal posterior sulcus. See the legend of Fig. 5 for the list of explored regions and corresponding electrode names.

The SEEG recordings contained 163 monopolar signals (sampling rate = 1024 Hz, skull reference). For simplicity, Fig. 5.C shows the patient's typical interictal activity (20 s epoch). 64 bipolar signals are displayed because they exhibit prominent epileptic spikes and spike-waves.

As shown in Fig. 5.C, a subset of 7 signals (TP5-6, A8-9, B9-10, TB8-9, T7-8, H8-9, DYS1-2) was selected based on the epileptogenicity index (EI, (Bartolomei et al., 2008)) values. For each channel, tens of epileptic spikes were averaged to obtain a prototypical epileptiform event (Fig. 6.B, red traces). These averaged waveforms illustrate the wide variety of spikes and spike-waves recorded in the EZ (red disk, EI = 1) and in the connected PZs (green disks, EI < 0.6).

Simulated epileptic spikes and spike-waves (Fig. 6, black traces) were then obtained by manually tuning the model parameters, as represented next to the averaged recorded epileptic spikes and

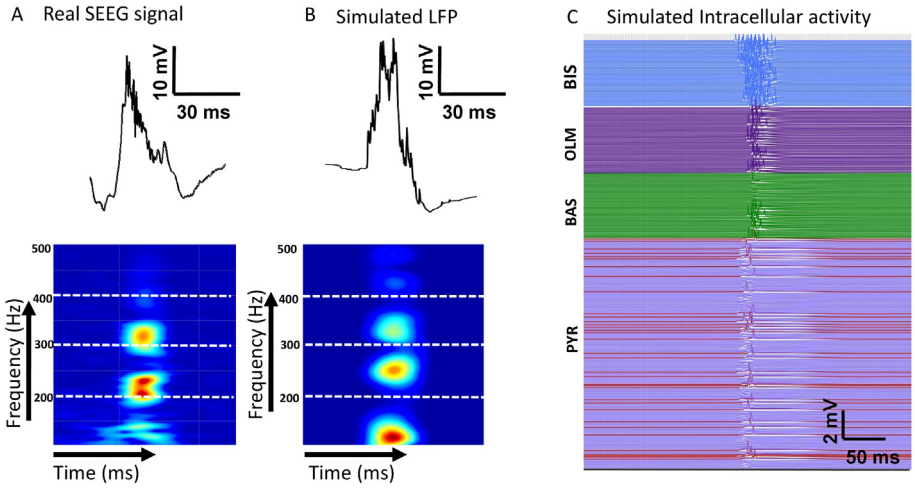


**Fig. 4.** Example of simulation results obtained with the microscale model. A, top) Real high frequency oscillation (HFO) recorded during SEEG exploration (electrode contact positioned in the hippocampus). A, bottom) Time-frequency representation (spectrogram) showing the presence of signal energy in the [200–300] Hz frequency band, typical of epileptic fast ripples (FRs). B) Simulated fast ripple (top) and corresponding spectrogram (bottom) showing the similarity to real FRs. C) Simulated intracellular activity of Glutamatergic principal neurons (PYR: pyramidal cells) and in GABAergic interneurons (BAS: basket cells; OLM: oriens lacunosom/moleculare cells, BIS: bistratified cells). The high frequency component (>300 Hz) is explained by weakly synchronized action potentials generated by small clusters of PYRs characterized by increased excitation.

spike-waves (Fig. 6, red traces). The global analysis of the simulation results revealed that the model was able to reproduce specific waveforms of interictal events observed in real SEEG signals with excellent accuracy (in terms of face value) considering their complexity (monophasic spikes and biphasic spike-waves, sharpness of the spike component, duration of the wave component).

In addition, the model provided insights into the mechanisms underlying the spike and the wave components of the actual spike-waves, as well as the time delay between the two components.

First, the model showed that the initial spike component was generated in two loops involving PYR cells and both SST + and PV + interneurons. More specifically, sharp spikes resulted from co-occurring GLU and GABA synaptic currents generated at the level of somatic synapses (presence of $GABA_{a,fast}$ receptors). The sharpness was explained by the rise and decay time constants of corresponding EPSPs and IPSPs and their degree of synchronization.

Second, regarding the post-peak wave component, we found that spike-waves with longer-duration waves occurred more frequently in PZs. The model suggested that this component is generated in the PYR-SST + loop and is caused by GABAergic currents generated at apical synapses of PYR cells where $GABA_{a,slow}$ receptors are implemented.

Third, the model revealed that both the wave duration and the delay between the spike and the wave components were explained by the rise and decay time constants of IPSPs generated by PYR cells in response to input from INs. Interestingly, the interictal epileptic discharges (IEDs) recorded in the EZ displayed sharper spikes and shorter delays between the fast spike and slow wave components. As explained by the model, GABAergic interneurons receive strong and brief excitatory inputs from local PYR cells and generate synchronized responses. IEDs with sharper spikes generated in the EZ are due to strong synchronization and fast response of basal GABAergic INs. IEDs with longer spike-wave delays observed in PZs are due to prolonged excitatory inputs to GABAergic INs and longer and delayed IPSPs.

Finally, as shown in Fig. 6.B, the model could accurately reproduce interictal epileptic spikes and spike-waves recorded in the EZ near a focal cortical dysplasia located in the temporal posterior sulcus (electrode contacts DYS2-3) separating the superior temporal gyrus and the middle temporal gyrus (electrode contacts T7-8). These realistic spike-waves generated in the dysplasia could be obtained for increased levels of GLU excitation and decreased levels of dendritic GABAergic inhibition. Regarding the PZs (green circles), although the E/I ratio was augmented compared to that of "normal NMs", spike-waves were not generated spontaneously but were caused by the excitatory input from the EZ.

### *3.3. Whole brain modeling predicts scalp-EEG signals from the topography and dynamics of intracerebral sources*

In this section, we report simulation results obtained from the whole brain model personalized from MRI and SEEG/EEG data recorded in the same patient, as described in 3.2.

CT scan images indicating the localization of the intracerebral electrodes are provided in Fig. 5.A with electrode names and recorded brain regions.

Interictal epileptic spikes and spike-waves were recorded in the EZ close to a focal cortical dysplasia located in the temporal posterior sulcus (electrode contacts DYS2 and DYS3) separating the superior temporal gyrus (STG) and the middle temporal gyrus (MTG) (electrode contacts T8 and T9).

Firstly, parameters of the interconnected NMMs included in the whole-brain model were set to generate normal EEG activity, except for epileptic activity, for which parameter values were fitted from the signal recorded at electrode DYS2-3 (located in the EZ). Then, the functional connectivity between the EZ and PZ as well as their position and spatial extent were optimized based on the matching of simulated and real scalp EEG signals (quantified by the cross-correlation function). Regarding the functional connectivity, values were increased between EZ and PZ but were decreased between EZ and healthy brain regions. Regarding the spatial extent, the triangular facets of the 3D cortical mesh were progressively aggregated to define the EZ. A similar procedure was used to tune the surface of the PZ.

Next, the EEG forward problem was solved to calculate the electrical contribution of the EZ and the PZ at the electrodes positioned on the scalp. The results of this process are shown in Fig. 7 for three different scenarios resulting in a mismatch between real EEG signals (Fig. 7.A) and simulated signals (Fig. 7.B, 7.C, 7.D). The first scenario (Fig. 7.B) showed that too small areas of EZ and PZ lead to

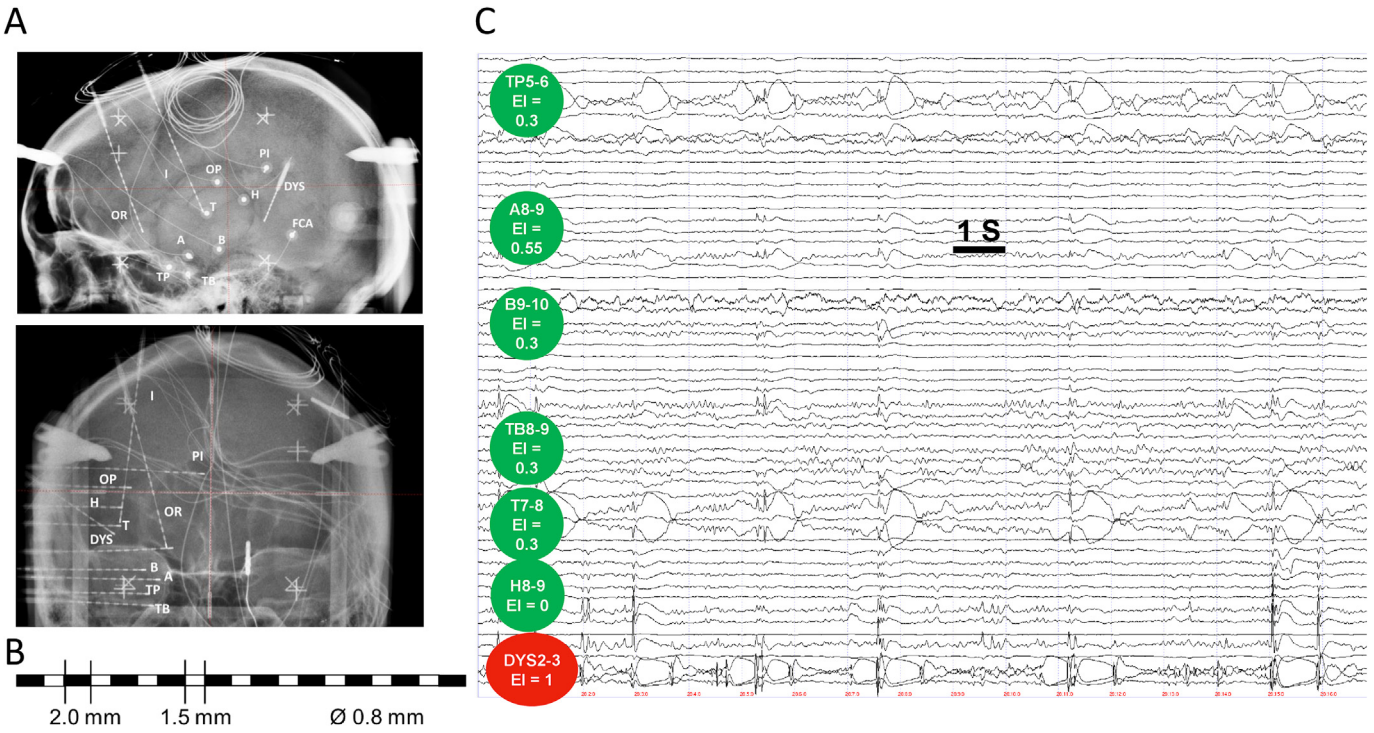


**Fig. 5.** Stereoelectroencephalographic (SEEG) exploration in a patient with lateral temporal lobe epilepsy. A) Sagittal and coronal CT-scan views showing the depth-EEG electrodes implanted in a perpendicular or oblique direction with respect to the brain surface. Electrode names refer to the following recorded regions: OR: fronto-orbital, OP: parieto-opercular, PI: sub-parietal, A: amygdala, TP: temporal pole, TB: temporo-basal cortex, H: Heschl gyrus, B: hippocampus, FCA: anterior fissura calcarina, Superior Temporal gyrus: T, DYS: dysplasia. B) Schematic diagram of a multi-contact intracerebral electrode. C) A 15-second epoch of SEEG recording with focus on bipolar channels of interest (colored disks) with corresponding Epileptogenicity Index (EI) values calculated from seizures (Bartolomei et al., 2008).

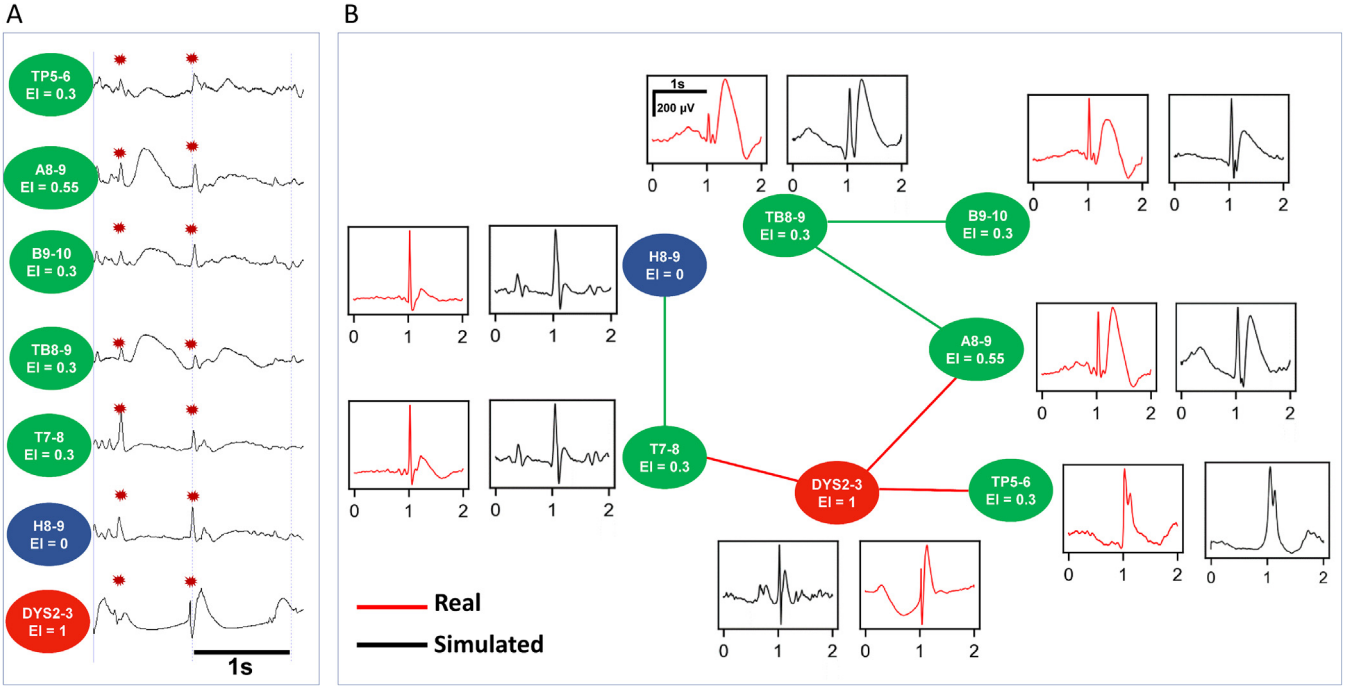


**Fig. 6.** Interictal network identified from SEEG recordings. Each node represents a bipolar SEEG channel in a brain region with epileptogenicity index (EI) values (Bartolomei et al., 2008) calculated from seizures. The red ellipse denotes the epileptogenic zone (EI = 1), the green ellipse corresponds to propagation zones (EI < 0.6) and the blue ellipse denotes a healthy brain region (EI = 0). A) Magnified view of intracerebral activity recorded during typical interictal events. B) Average waveforms of detected epileptic spikes and spikes waves on each bipolar channel in the patient (red traces) along with simulated signals (black traces).

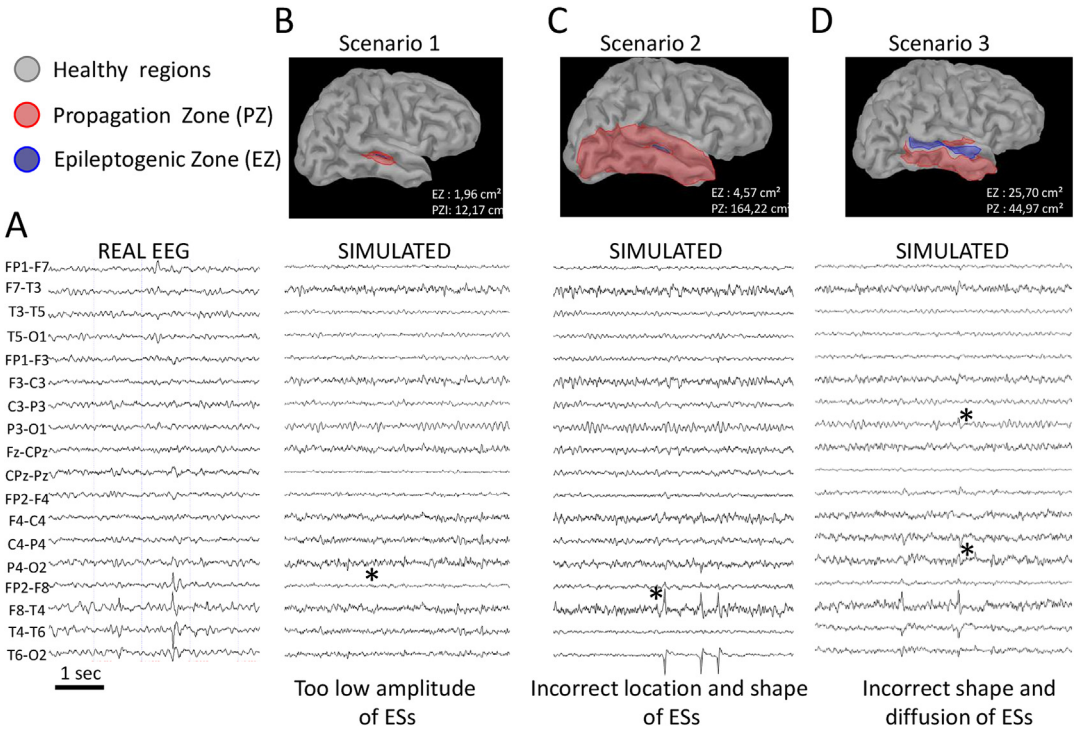


**Fig. 7.** Simulation of scalp EEG signals using the large-scale model (whole brain). A) Short epoch of real EEG signals disclosing epileptic spikes (ESs) generated in the right hemisphere (temporal and central regions). B) Simulated EEG for a first scenario on the model parameter configuration in which the surface of the epileptic zone (EZ) and the propagation zone (PZ) are too small, resulting in very low amplitude epileptic spikes that differ from real ones. C) In the second scenario where the extension of the PZ is large, simulated EEG epileptic spikes do not match real ones in terms of location (no spike inversion at T4-T6) and waveform (large and sharp spikes at T6-O2). D) Simulated EEG for a third scenario where the position of the EZ and PZ is incorrect, resulting in simulated epileptic spikes (ESs) which do not match the real ones in terms of waveform and topography.

incorrect amplitude of interictal epileptic spikes (ESs) at the scalp level. In contrast, the second scenario (Fig. 7.C) indicated that incorrect spatial extension of the PZ leads to incorrect location and shape of epileptic spikes. Similarly, the third scenario (Fig. 7. D) demonstrated that an inaccurate position of the EZ and PZ resulted in a diffusion of epileptic spikes that did not resemble those actually recorded at the scalp level.

These results show that the parameter tuning process must obey strict constraints to obtain an accurate matching between simulated and real scalp EEG signals. As shown in Fig. 8, such similarity could only be achieved for well-defined position and spatial extent of EZ and PZ. As depicted on EEG signals (Fig. 8.A), the simulated interictal ESs closely reproduced (correct amplitude, polarity and localization (F8-T4, T4-P8 and P8-O2)) those actually recorded for optimal tuning of the model parameters. Importantly, the prediction of the model in terms of EZ and PZ localization and spatial extent was confirmed by the post-surgical result. As shown in Fig. 8.B (middle and right panels), the resected region, which included the EZ and a large part of the PZ, resulted in the complete disappearance of seizures (Engel class 1).

## 4. Discussion

The purpose of this research article is to provide a global overview of computational hybrid models reflecting physical and physiological mechanisms that are useful for interpreting intracerebral and scalp EEG data recorded during interictal periods in patients with epilepsy. These models were developed at three different levels of description and provide insightful information about the mechanisms underlying epileptiform events (fast ripples, epileptic spikes, and spike-waves) commonly observed in patients outside seizures. In this regard, they differ from more abstract phenomenological models (El Houssaini et al., 2020), also developed in the context of epilepsy, which are based on mathematical equations more loosely connected to neuronal physiology.

The key findings are summarized below and then discussed in the sections that follow.

First, the three model types demonstrated substantial integrative value. They provided an effective way to i) articulate neurobiological and neurophysiological insights into neural networks comprising major types of glutamatergic pyramidal cells and GABAergic interneurons and ii) integrate pathophysiological changes at cellular and network levels to reproduce epileptiform events observed in electrophysiological signals.

Second, for the three levels of description, the models presented showed a high ability to accurately reproduce observed epileptiform events (so-called *face value* (Suffczynski et al., 2006)) not only because they are based on neurophysiological data but also because they integrate a factual reconstruction of electrophysiological signals (LFPs, SEEG and scalp EEG) grounded in biophysical principles such as the effect of monopolar or dipolar behavior of neuronal sources as predicted by electromagnetism.

Third, they were found to have a high explanatory value, providing valuable insights into the mechanisms underlying the generation of high-frequency oscillations (fast ripples) and interictal spikes and spike-waves, observed in intracerebral and scalp EEG recordings of patients.

*Microscale model*. Regarding the generation of fast ripples in the hippocampus, our microscale model confirmed that an external excitatory input to the CA1 subfield, likely originating from CA3, is necessary to reproduce the slow component with superimposed fast oscillations. This result is consistent with a number of studies including (Nunez-Ochoa et al., 2021, Ortiz et al., 2018) which

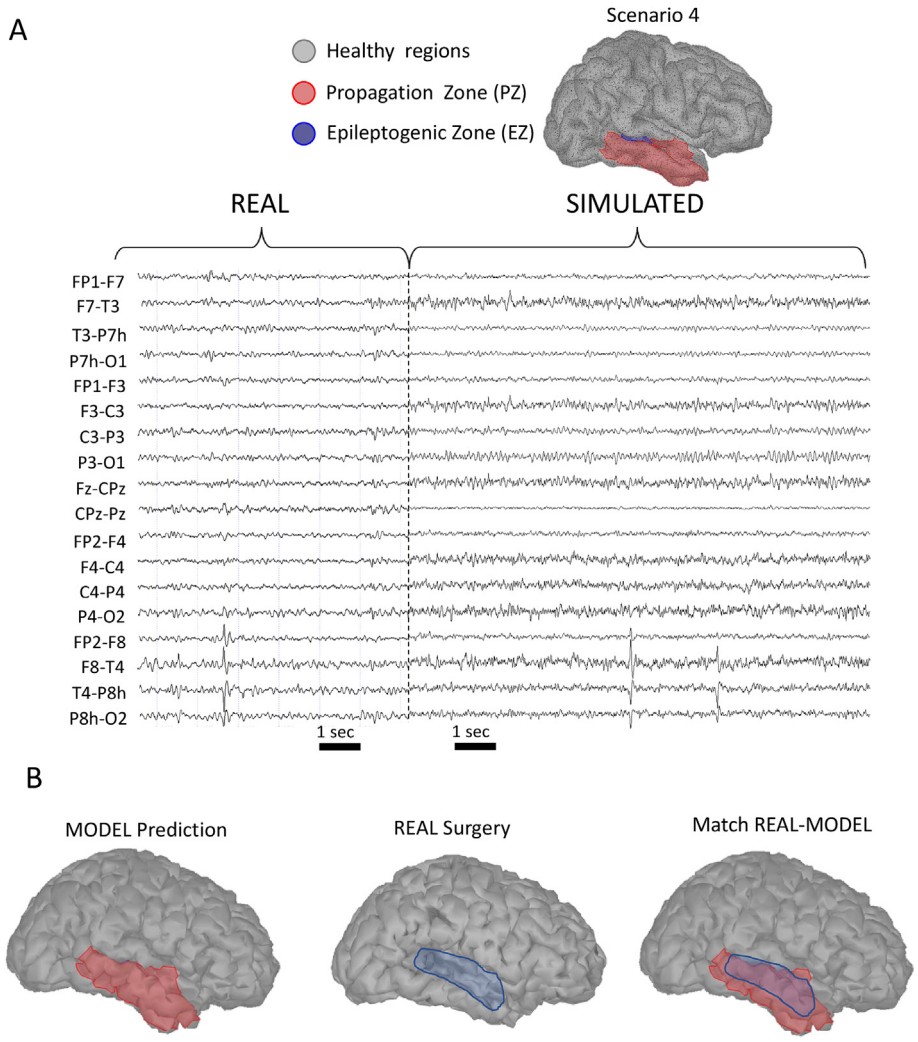


**Fig. 8.** Comparison between real and simulated scalp EEG signals. A) For optimal tuning of EZ and PZ parameters in the large-scale model, simulated epileptic spikes strongly resemble real spikes in terms of topography (channels F8-T4, T4-P8h, P8h-O2), polarity and waveforms. B) Model prediction (left) regarding the spatial extent of the epileptogenic zone (EZ) and the propagation zone (PZ) along with the resection actually performed (middle) and the superposition of predicted and resected zones (right).

provided *in vitro* evidence that fast ripple events in CA1 are initiated by CA3 multiunit activity. It is noteworthy that the high-frequency oscillatory component is in the range of [200–600] Hz, which is well above the maximum firing rate of CA1 pyramidal cells (about 40–50 Hz) (Avignone et al., 2005). The model could explain this difference by the fact that the observed very fast oscillation is due to pyramidal cell firing patterns contributing in a weakly synchronized manner to the local field potential recorded extracellularly by the (relatively large) electrode.

This finding is in agreement with those reported by Foffani et al. (Foffani et al., 2007) showing that HFOs may reflect a pathological desynchronization of the normal ripple pattern. More precisely, the out-of-phase bursting of PYR cells would result in emergent FRs (Ibarz et al., 2010). From a computational modeling perspective, this corroborates the analysis of Fink and colleagues (Fink et al., 2015) who also found that abnormal ripples arise when input to pyramidal cells overcomes network inhibition, resulting in high-frequency uncoordinated firing. Interestingly, our model was able to generate realistic fast ripples (FRs, [200–600 Hz]) without integrating axon-axon gap junctions between pyramidal neurons. In this respect, it differs from those described by Traub and colleages (Traub and Bibbig, 2000, Traub et al., 1999) where the fast oscillation is generated by electrically coupled pyramidal cell axons, leading to phasic excitation of interneurons at ripple frequency.

*Mesoscale model.* Regarding the generation of interictal ESs and SWs in neocortical brain regions, our results strongly suggest that mesoscale neurophysiological layered models of neural masses are very well suited to approximate simple and more complex waveforms of epileptiform events recorded with SEEG outside seizures. This result demonstrates the high variability of electrographic manifestation of IEDs, with distinct subtypes of SWs depending on lamina-selective disinhibition or enhanced interlaminar excitation, as suggested in (Hall et al., 2018). More specifically, we proposed a novel layered neuronal population model that considers synaptically connected subpopulations of PYR cells and GABAergic INs spatially distributed across the 6 layers of the human neocortex. To our knowledge, this modeling approach, recently presented by our group (Koksal-Ersoz et al., 2022, Lopez-Sola et al., 2022), has not been reported elsewhere.

According to this model, connections between neuronal subpopulations play a crucial role in generating realistic SWs through synaptic mechanisms. The spike component of SWs is glutamatergic (PYR-PYR collateral excitation), while the wave component is GABAergic (PYR-SST + circuit). This result is consistent with previous experimental (Cossart et al., 2005, Huneau et al., 2013, Yekhlef et al., 2015) and computational modeling studies (Demont-Guignard et al., 2012, Ratnadurai-Giridharan et al., 2014, Wendling et al., 2002) which have shown that the epileptogenicity

of neuronal populations can be explained by the alteration of the input of SST + INs to GABAa receptors of PYR cells. In this particular circuit, EPSPs and IPSPs are generated at the level of basal and apical dendritic synapses. Indeed, in contrast to our previous model for the hippocampus (Geng and Zhou, 2016, Wendling et al., 2002), INs target GABAa receptors of PYR cells in both superficial and deep layers of the neocortical column with different physiologically plausible IPSP kinetics. Our results show that a better approximation of the various waveforms of IEDs observed in SEEG (from simple monophasic spikes to more complex biphasic spike-waves) can be obtained by using two monopoles in opposite directions for the reconstruction of signals recorded at the level of intracerebral electrode contacts. This biophysical consideration was based on the description of current flow patterns within and around an idealized neuron in response to synaptic activation which creates active sources and passive sinks at the basal and distal dendrites depending on the excitatory or inhibitory input (Lopes da Silva, 2011).

Regarding the interpretation of IED waveforms, the model provided insight into subtle differences in the morphology of SWs in terms of the sharpness of the spike component, the duration of the wave component and the delay between the spike and the wave. Specifically, by reducing glutamatergic signaling in the PYR cell subpopulation, we were able to increase the spike duration (i.e., reduce the spike sharpness) and to obtain a long-lasting inhibition that increased the spike/wave delay and the wave duration. Interestingly, in the model, these sharpless spikes with delayed longer waves are being generated in non-epileptogenic zones (NEZs). This finding suggests that inhibition is still functional in NEZs where "green spikes" are being generated in response to excitatory input from epileptogenic zones (EZs) that produce "red spikes" (sharp spikes followed by short waves). It also confirms the study reported by Serafini (Serafini, 2019), which concluded that green spikes have more pronounced slow waves than red spikes and that peripheral slow-wave amplitudes correlate with seizure suppression due to preserved surrounding inhibition.

*Macroscale model*. Regarding the macroscopic level of description, our results show that the whole-brain computational model we previously developed for consciousness studies (Bensaid et al., 2019) can also provide insightful information about IEDs recorded in scalp EEG signals. The model we developed is adapted to the patient-specificity of epileptiform activity originating from neocortical brain sources and reflected in EEG signals collected from electrodes positioned on the patient's head. Our approach builds on the neuronal population model adapted to the neocortex (Appendix B) and extends the single neural mass to a network of spatially distributed interconnected neural masses (Appendix C). In a similar approach (van Nifterick et al., 2022), the authors made use of a whole-brain computational network model comprising of 78 neural masses coupled according to structural brain topology in order to link neural hyperactivity underlying the E/I imbalance to brain network dysfunction in early Alzheimer disease. In the context of epilepsy, seizure propagation patterns have been analyzed using a model comprising 88 nodes equipped with region-specific neural mass models capable of simulating a range of epileptiform discharges (Olmi et al., 2019). Along the same line, but from a more theoretical viewpoint, mechanisms of epileptic states and state transitions were studied using a network model composed of coupled oscillatory units (Kalitzin et al., 2019). Nevertheless, our model differs from those presented elsewhere as the large-scale brain network includes neural masses in which neuronal mechanisms are neurophysiologically grounded. To our knowledge, this feature is unique and provides an opportunity to bridge neocortical regional microcircuitry with whole-brain macrocircuitry. Using this approach, we were able to simulate realistic scalp EEG signals comprising interictal ESs and SWs that matched those actually recorded in the patient. Interestingly, this approach led to the identification of the patient-specific epileptogenic zone (EZ) and propagation zone (PZ). To proceed, we used a visual iterative procedure in which the tuning of parameters related to epileptic sources minimizes the distance between real and simulated epileptic spikes in terms of involved EEG channels (topography), amplitude and polarity of patterns. Given the number of adjustable parameters, one might expect that a multitude of possible combinations could lead to plausible EEG signals. However, our findings reveal a contrasting result: the stringent spatio-temporal constraints are such that only a few combinations yield EEG signals similar to patient-specific signals with significant clinical value. In this regard, the EZ identified by the model was part of the area resected in the patient, who is now seizure-free two years after surgery. This result confirms those reported in recent studies suggesting that brain models could be used in the pre-surgical evaluation of patients to tailor neurosurgery (An et al., 2019, Lang et al., 2023).

Overall, for the three levels of description, fine-tuning of the free parameters and quantitative comparison with real data allowed us to reproduce interictal epileptic events with a high degree of realism and to formulate hypotheses about the cell- and network-related mechanisms underlying the generation of FRs and IEDs observed in SEEG signals.

Overcoming the limitations of the proposed approach will strengthen these positive results. Firstly, the tuning of model parameters is based on visual comparison of simulated and real signals supported by graphical user interfaces the speed up the search for optimal values. However, this process is still time-consuming, and automatic methods for identifying model parameters will be useful. More specifically, one approach based on evolutionary algorithms (Dunstan et al., 2023, Wendling et al., 2005) will be considered for mapping NMM parameters. Second, regarding the macroscale model, improvements can also be achieved by including subcortical structures in the 3D brain mesh in addition to neocortical regions. This extension would allow further investigation of scalp EEG signals generated by epileptogenic networks involving deep brain regions such as the amygdala or the hippocampus, among others. Finally, future work will also investigate the ability of the proposed models to predict optimized therapeutic strategies based on neurostimulation and neuromodulation. Regarding resection strategies, the field of personalized whole-brain modeling is advancing rapidly, and neurosurgical applications of this technology can provide support for clinical decision-making (Dallmer-Zerbe et al., 2023, Lang et al., 2023). Similarly, such individualized models can provide guidance for the optimization of neurostimulation and neuromodulation interventions. Overall, this study highlights the high potential of hybrid computational modeling combining (patho)physiological mechanisms with physical principles for clinical epileptology.

## CRediT authorship contribution statement

**Fabrice Wendling:** Conceptualization, Methodology, Formal analysis, Validation, Visualization, Funding acquisition. **Elif Koksal-Ersoz:** Data curation, Methodology, Formal analysis, Validation, Visualization, Software. **Mariam Al-Harrach:** Data curation, Methodology, Formal analysis, Validation, Visualization, Software. **Maxime Yochum:** Software. **Isabelle Merlet:** Formal analysis, Validation, Visualization. **Giulio Ruffini:** Conceptualization, Funding acquisition. **Fabrice Bartolomei:** Conceptualization, Funding acquisition. **Pascal Benquet:** Data curation, Methodology, Formal analysis, Validation, Visualization.

## Acknowledgement

This project has received funding from the European Research Council (ERC) under the European Union's Horizon 2020 research and innovation program (Grant Agreement No. 855109).

## Declarations of interest

None.

## Appendix A. Supplementary data

Supplementary data to this article can be found online at https://doi.org/10.1016/j.clinph.2024.03.006.

## References

Adler DH, Liu AY, Pluta J, Kadivar S, Orozco S, Wang H, et al. Reconstruction of the Human Hippocampus in 3d from Histology and High-Resolution Ex-Vivo Mri. Proc IEEE Int Symp Biomed Imaging 2012;2012:294–7.
An S, Bartolomei F, Guye M, Jirsa V. Optimization of surgical intervention outside the epileptogenic zone in the Virtual Epileptic Patient (VEP). PLoS Comput Biol 2019;15(6) e1007051.
Aronica E, Muhlebner A. Neuropathology of epilepsy. Handb Clin Neurol 2017;145:193–216.
Avignone E, Frenguelli BG, Irving AJ. Differential responses to NMDA receptor activation in rat hippocampal interneurons and pyramidal cells may underlie enhanced pyramidal cell vulnerability. Eur J Neurosci 2005;22(12):3077–90.
Bancaud J, Angelergues R, Bernouilli C, Bonis A, Bordas-Ferrer M, Bresson M, et al. Functional stereotaxic exploration (SEEG) of epilepsy. Electroencephalogr Clin Neurophysiol 1970;28(1):85–6.
Bartolomei F, Chauvel P, Wendling F. Epileptogenicity of brain structures in human temporal lobe epilepsy: a quantified study from intracerebral EEG. Brain 2008;131(Pt 7):1818–30.
Bartolomei F, Lagarde S, Wendling F, McGonigal A, Jirsa V, Guye M, et al. Defining epileptogenic networks: Contribution of SEEG and signal analysis. Epilepsia 2017;58(7):1131–47.
Belperio G, Corso C, Duarte CB, Mele M. Molecular mechanisms of epilepsy: the role of the chloride transporter KCC2. J Mol Neurosci 2022;72(7):1500–15.
Bensaid S, Modolo J, Merlet I, Wendling F, Benquet P. COALIA: A computational model of human EEG for consciousness research. Front Syst Neurosci 2019;13:59.
Binnie CD, Stefan H. Modern electroencephalography: its role in epilepsy management. Clin Neurophysiol 1999;110(10):1671–97.
Bragin A, Engel Jr J, Wilson CL, Fried I, Buzsaki G. High-frequency oscillations in human brain. Hippocampus 1999a;9(2):137–42.
Bragin A, Engel Jr J, Wilson CL, Fried I, Mathern GW. Hippocampal and entorhinal cortex high-frequency oscillations (100–500 Hz) in human epileptic brain and in kainic acid–treated rats with chronic seizures. Epilepsia 1999b;40(2):127–37.
Bragin A, Engel Jr J, Wilson CL, Vizentin E, Mathern GW. Electrophysiologic analysis of a chronic seizure model after unilateral hippocampal KA injection. Epilepsia 1999c;40(9):1210–21.
Burman RJ, Selfe JS, Lee JH, van den Berg M, Calin A, Codadu NK, et al. Excitatory GABAergic signalling is associated with benzodiazepine resistance in status epilepticus. Brain 2019;142(11):3482–501.
Case M, Soltesz I. Computational modeling of epilepsy. Epilepsia 2011;52(Suppl 8 (Suppl 8)):12–5.
Casillas-Espinosa PM, Powell KL, O'Brien TJ. Regulators of synaptic transmission: roles in the pathogenesis and treatment of epilepsy. Epilepsia 2012;53(Suppl 9):41–58.
Catterall WA. Sodium Channel Mutations and Epilepsy. In: Noebels JL, Avoli M, Rogawski MA, Olsen RW, Delgado-Escueta AV, editors. Jasper's Basic Mechanisms of the Epilepsies. 4th ed. Bethesda (MD); 2012.
Colciaghi F, Finardi A, Nobili P, Locatelli D, Spigolon G, Battaglia GS. Progressive brain damage, synaptic reorganization and NMDA activation in a model of epileptogenic cortical dysplasia. PLoS One 2014;9(2):e89898.
Cosandier-Rimele D, Merlet I, Bartolomei F, Badier JM, Wendling F. Computational modeling of epileptic activity: from cortical sources to EEG signals. J Clin Neurophysiol 2010;27(6):465–70.
Cossart R, Bernard C, Ben-Ari Y. Multiple facets of GABAergic neurons and synapses: multiple fates of GABA signalling in epilepsies. Trends Neurosci 2005;28(2):108–15.
Cuello-Oderiz C, von Ellenrieder N, Sankhe R, Olivier A, Hall J, Dubeau F, et al. Value of ictal and interictal epileptiform discharges and high frequency oscillations for delineating the epileptogenic zone in patients with focal cortical dysplasia. Clin Neurophysiol 2018;129(6):1311–9.
Dallmer-Zerbe I, Jiruska P, Hlinka J. Personalized dynamic network models of the human brain as a future tool for planning and optimizing epilepsy therapy. Epilepsia 2023.
de Curtis M, Avanzini G. Interictal spikes in focal epileptogenesis. Prog Neurobiol 2001;63(5):541–67.
de Curtis M, Jefferys JGR, Avoli M. Interictal Epileptiform Discharges in Partial Epilepsy: Complex Neurobiological Mechanisms Based on Experimental and Clinical Evidence. In: Noebels JL, Avoli M, Rogawski MA, Olsen RW, Delgado-Escueta AV, editors. Jasper's Basic Mechanisms of the Epilepsies. 4th ed. Bethesda (MD); 2012.
de Curtis M, Uva L, Gnatkovsky V, Librizzi L. Potassium dynamics and seizures: Why is potassium ictogenic? Epilepsy Res 2018;143:50–9.
Demont-Guignard S, Benquet P, Gerber U, Biraben A, Martin B, Wendling F. Distinct hyperexcitability mechanisms underlie fast ripples and epileptic spikes. Ann Neurol 2012;71(3):342–52.
Demont-Guignard S, Benquet P, Gerber U, Wendling F. Analysis of intracerebral EEG recordings of epileptic spikes: insights from a neural network model. IEEE Trans Biomed Eng 2009;56(12):2782–95.
Desikan RS, Segonne F, Fischl B, Quinn BT, Dickerson BC, Blacker D, et al. An automated labeling system for subdividing the human cerebral cortex on MRI scans into gyral based regions of interest. Neuroimage 2006;31(3):968–80.
Dichter MA. Cellular mechanisms of epilepsy and potential new treatment strategies. Epilepsia 1989;30(5):S3–S12. discussion S64-8.
Dunstan DM, Richardson MP, Abela E, Akman OE, Goodfellow M. Global nonlinear approach for mapping parameters of neural mass models. PLoS Comput Biol 2023;19(3):e1010985.
El Houssaini K, Bernard C, Jirsa VK. The epileptor model: a systematic mathematical analysis linked to the dynamics of seizures, refractory status epilepticus, and depolarization block. eNeuro 2020;7(2).
El Youssef N, Jegou A, Makhalova J, Naccache L, Benar C, Bartolomei F. Consciousness alteration in focal epilepsy is related to loss of signal complexity and information processing. Sci Rep 2022;12(1):22276.
Eyal G, Verhoog MB, Testa-Silva G, Deitcher Y, Benavides-Piccione R, DeFelipe J, et al. Human Cortical Pyramidal Neurons: From Spines to Spikes via Models. Front Cell Neurosci 2018;12:181.
Fabo D, Bokodi V, Szabo JP, Toth E, Salami P, Keller CJ, et al. The role of superficial and deep layers in the generation of high frequency oscillations and interictal epileptiform discharges in the human cortex. Sci Rep 2023;13(1):9620.
Fink CG, Gliske S, Catoni N, Stacey WC. Network mechanisms generating abnormal and normal hippocampal high-frequency oscillations: A Computational Analysis. eNeuro 2015;2(3).
Foffani G, Uzcategui YG, Gal B, Menendez de la Prida L. Reduced spike-timing reliability correlates with the emergence of fast ripples in the rat epileptic hippocampus. Neuron 2007;55(6):930–41.
Freeman WJ. Models of the dynamics of neural populations. Electroencephalogr Clin Neurophysiol Suppl 1978;34:9–18.
Geng S, Zhou W. Influence of extrinsic inputs and synaptic gains on dynamics of Wendling's neural mass model: A bifurcation analysis. J Integr Neurosci 2016;15(4):463–83.
Gentiletti D, de Curtis M, Gnatkovsky V, Suffczynski P. Focal seizures are organized by feedback between neural activity and ion concentration changes. Elife 2022;11.
Hagmann P, Cammoun L, Gigandet X, Meuli R, Honey CJ, Wedeen VJ, et al. Mapping the structural core of human cerebral cortex. PLoS Biol 2008;6(7):e159.
Hajos M, Hoffmann WE, Orban G, Kiss T, Erdi P. Modulation of septo-hippocampal Theta activity by GABAA receptors: an experimental and computational approach. Neuroscience 2004;126(3):599–610.
Hall SP, Traub RD, Adams NE, Cunningham MO, Schofield I, Jenkins AJ, et al. Enhanced interlaminar excitation or reduced superficial layer inhibition in neocortex generates different spike-and-wave-like electrographic events in vitro. J Neurophysiol 2018;119(1):49–61.
Hedrick TP, Nobis WP, Foote KM, Ishii T, Chetkovich DM, Swanson GT. Excitatory synaptic input to hilar mossy cells under basal and hyperexcitable conditions. eNeuro 2017;4(6).
Huberfeld G, Wittner L, Clemenceau S, Baulac M, Kaila K, Miles R, et al. Perturbed chloride homeostasis and GABAergic signaling in human temporal lobe epilepsy. J Neurosci 2007;27(37):9866–73.
Huneau C, Benquet P, Dieuset G, Biraben A, Martin B, Wendling F. Shape features of epileptic spikes are a marker of epileptogenesis in mice. Epilepsia 2013;54(12):2219–27.
Ibarz JM, Foffani G, Cid E, Inostroza M. Menendez de la Prida L. Emergent dynamics of fast ripples in the epileptic hippocampus. J Neurosci 2010;30(48):16249–61.
Isnard J, Taussig D, Bartolomei F, Bourdillon P, Catenoix H, Chassoux F, et al. French guidelines on stereoelectroencephalography (SEEG). Neurophysiol Clin 2018;48(1):5–13.
Jacobs J, Levan P, Chatillon CE, Olivier A, Dubeau F, Gotman J. High frequency oscillations in intracranial EEGs mark epileptogenicity rather than lesion type. Brain 2009;132(Pt 4):1022–37.
Jiruska P, Alvarado-Rojas C, Schevon CA, Staba R, Stacey W, Wendling F, et al. Update on the mechanisms and roles of high-frequency oscillations in seizures and epileptic disorders. Epilepsia 2017;58(8):1330–9.
Kalitzin S, Petkov G, Suffczynski P, Grigorovsky V, Bardakjian BL, Lopes da Silva F, et al. Epilepsy as a manifestation of a multistate network of oscillatory systems. Neurobiol Dis 2019;130 104488.
Keller CJ, Truccolo W, Gale JT, Eskandar E, Thesen T, Carlson C, et al. Heterogeneous neuronal firing patterns during interictal epileptiform discharges in the human cortex. Brain 2010;133(Pt 6):1668–81.

Koksal-Ersoz E, Lazazzera R, Yochum M, Merlet I, Makhalova J, Mercadal B, et al. Signal processing and computational modeling for interpretation of SEEG-recorded interictal epileptiform discharges in epileptogenic and non-epileptogenic zones. J Neural Eng 2022;19(5).
Lang S, Momi D, Vetkas A, Santyr B, Yang AZ, Kalia SK, et al. Computational modeling of whole-brain dynamics: a review of neurosurgical applications. J Neurosurg 2023:1–13.
Lariviere S, Royer J, Rodriguez-Cruces R, Paquola C, Caligiuri ME, Gambardella A, et al. Structural network alterations in focal and generalized epilepsy assessed in a worldwide ENIGMA study follow axes of epilepsy risk gene expression. Nat Commun 2022;13(1):4320.
Levesque M, Avoli M. High-frequency oscillations and focal seizures in epileptic rodents. Neurobiol Dis 2019;124:396–407.
Liu R, Wang J, Liang S, Zhang G, Yang X. Role of NKCC1 and KCC2 in Epilepsy: From Expression to Function. Front Neurol 2019;10:1407.
Lopes da Silva FH. Biophysical Aspects of EEG and Magnetoencephalogram Generation. in Niedermeyer's Electroencephalography: Basic Principles, Clinical Applications, and Related Fields, Edited by Schomer, DL and Lopes da Silva, 6th edition 2011.
Lopes da Silva FH, Hoeks A, Smits H, Zetterberg LH. Model of brain rhythmic activity. The alpha-rhythm of the thalamus. Kybernetik 1974;15(1):27–37.
Lopez-Sola E, Sanchez-Todo R, Lleal E, Koksal-Ersoz E, Yochum M, Makhalova J, et al. A personalizable autonomous neural mass model of epileptic seizures. J Neural Eng 2022;19(5).
Makhalova J, Medina Villalon S, Wang H, Giusiano B, Woodman M, Benar C, et al. Virtual epileptic patient brain modeling: Relationships with seizure onset and surgical outcome. Epilepsia 2022;63(8):1942–55.
Markram H, Muller E, Ramaswamy S, Reimann MW, Abdellah M, Sanchez CA, et al. Reconstruction and Simulation of Neocortical Microcircuitry. Cell 2015;163(2):456–92.
Mina F, Benquet P, Pasnicu A, Biraben A, Wendling F. Modulation of epileptic activity by deep brain stimulation: a model-based study of frequency-dependent effects. Front Comput Neurosci 2013;7:94.
Molaee-Ardekani B, Benquet P, Bartolomei F, Wendling F. Computational modeling of high-frequency oscillations at the onset of neocortical partial seizures: from 'altered structure' to 'dysfunction'. Neuroimage 2010;52(3):1109–22.
Naylor DE, Liu H, Niquet J, Wasterlain CG. Rapid surface accumulation of NMDA receptors increases glutamatergic excitation during status epilepticus. Neurobiol Dis 2013;54:225–38.
Nemani VM, Binder DK. Emerging role of gap junctions in epilepsy. Histol Histopathol 2005;20(1):253–9.
Nunez-Ochoa MA, Chipres-Tinajero GA, Gonzalez-Dominguez NP, Medina-Ceja L. Causal relationship of CA3 back-projection to the dentate gyrus and its role in CA1 fast ripple generation. BMC Neurosci 2021;22(1):37.
Olmi S, Petkoski S, Guye M, Bartolomei F, Jirsa V. Controlling seizure propagation in large-scale brain networks. PLoS Comput Biol 2019;15(2):e1006805.
Ortiz F, Zapfe WPK, Draguhn A, Gutierrez R. Early Appearance and Spread of Fast Ripples in the Hippocampus in a Model of Cortical Traumatic Brain Injury. J Neurosci 2018;38(42):9034–46.
Pail M, Cimbalnik J, Roman R, Daniel P, Shaw DJ, Chrastina J, et al. High frequency oscillations in epileptic and non-epileptic human hippocampus during a cognitive task. Sci Rep 2020;10(1):18147.
Parker CS, Clayden JD, Cardoso MJ, Rodionov R, Duncan JS, Scott C, et al. Structural and effective connectivity in focal epilepsy. Neuroimage Clin 2018;17:943–52.
Ratnadurai-Giridharan S, Stefanescu RA, Khargonekar PP, Carney PR, Talathi SS. Genesis of interictal spikes in the CA1: a computational investigation. Front Neural Circuits 2014;8:2.
Romani A, Schurmann F, Markram H, Migliore M. Reconstruction of the Hippocampus. Adv Exp Med Biol 2022;1359:261–83.
Sanchez-Todo R, Bastos AM, Lopez-Sola E, Mercadal B, Santarnecchi E, Miller EK, et al. A physical neural mass model framework for the analysis of oscillatory generators from laminar electrophysiological recordings. Neuroimage 2023;270:119938.
Serafini R. Similarities and differences between the interictal epileptiform discharges of green-spikes and red-spikes zones of human neocortex. Clin Neurophysiol 2019;130(3):396–405.
Sinha N, Dauwels J, Kaiser M, Cash SS, Brandon Westover M, Wang Y, et al. Predicting neurosurgical outcomes in focal epilepsy patients using computational modelling. Brain 2017;140(2):319–32.
Staba RJ, Stead M, Worrell GA. Electrophysiological biomarkers of epilepsy. Neurotherapeutics : the journal of the American Society for Experimental NeuroTherapeutics 2014;11(2):334–46.
Staley KJ. Role of the depolarizing GABA response in epilepsy. Adv Exp Med Biol 2004;548:104–9.
Suffczynski P, Wendling F, Bellanger JJ, Da Silva FHL. Some insights into computational models of (patho)physiological brain activity. P Ieee 2006;94(4):784–804.
Swartz BE, Houser CR, Tomiyasu U, Walsh GO, DeSalles A, Rich JR, et al. Hippocampal cell loss in posttraumatic human epilepsy. Epilepsia 2006;47(8):1373–82.
Thomas J, Kahane P, Abdallah C, Avigdor T, Zweiphenning WJEM, Chabardes S, et al. A Subpopulation of Spikes Predicts Successful Epilepsy Surgery Outcome. Annals of Neurology 2023;93(3):522–35.
Thomson AM, Bannister AP. Interlaminar connections in the neocortex. Cereb Cortex 2003;13(1):5–14.
Touretzky D. Anatomy of the Hippocampus. In Computational Models of Neural Systems. Lecture 3.2. https://wwwcscmuedu/afs/cs/academic/class/15883-f19/slides/hc-anatomypdf 2019.
Traub RD, Bibbig A. A model of high-frequency ripples in the hippocampus based on synaptic coupling plus axon-axon gap junctions between pyramidal neurons. J Neurosci 2000;20(6):2086–93.
Traub RD, Schmitz D, Jefferys JG, Draguhn A. High-frequency population oscillations are predicted to occur in hippocampal pyramidal neuronal networks interconnected by axoaxonal gap junctions. Neuroscience 1999;92(2):407–26.
Urrestarazu E, Chander R, Dubeau F, Gotman J. Interictal high-frequency oscillations (100–500 Hz) in the intracerebral EEG of epileptic patients. Brain 2007;130(Pt 9):2354–66.
Van Essen D, Marcus D. Connectome Coordination Facility. www.humanconnectome.org; 2023. Available from: www.humanconnectome.org.
van Nifterick AM, Gouw AA, van Kesteren RE, Scheltens P, Stam CJ, de Haan W. A multiscale brain network model links Alzheimer's disease-mediated neuronal hyperactivity to large-scale oscillatory slowing. Alzheimers Res Ther 2022;14(1):101.
Volman V, Bazhenov M, Sejnowski TJ. Computational models of neuron-astrocyte interaction in epilepsy. Front Comput Neurosci 2012;6:58.
Wei YA, Nandi A, Jia XX, Siegle JH, Denman D, Lee SY, et al. Associations between in vitro, in vivo and in silico cell classes in mouse primary visual cortex. Nat Commun 2023;14(1).
Weiss SA, Staba RJ, Sharan A, Wu C, Rubinstein D, Das S, et al. Accuracy of high-frequency oscillations recorded intraoperatively for classification of epileptogenic regions. Sci Rep 2021;11(1):21388.
Wendling F, Bartolomei F, Bellanger JJ, Chauvel P. Epileptic fast activity can be explained by a model of impaired GABAergic dendritic inhibition. Eur J Neurosci 2002;15(9):1499–508.
Wendling F, Hernandez A, Bellanger JJ, Chauvel P, Bartolomei F. Interictal to ictal transition in human temporal lobe epilepsy: insights from a computational model of intracerebral EEG. J Clin Neurophysiol 2005;22(5):343–56.
Wilson HR, Cowan JD. Excitatory and inhibitory interactions in localized populations of model neurons. Biophys J 1972;12(1):1–24.
Yekhlef L, Breschi GL, Lagostena L, Russo G, Taverna S. Selective activation of parvalbumin- or somatostatin-expressing interneurons triggers epileptic seizurelike activity in mouse medial entorhinal cortex. J Neurophysiol 2015;113(5):1616–30.